Elsevier Editorial System(tm) for Journal of Molecular Biology
Manuscript Draft

Manuscript Number:

Title: Nucleotide-dependence of G-actin conformation from multiple molecular dynamics simulations and observation of a putatively polymerisation-competent superclosed state

Article Type: Full Length Article

Section/Category: Computational molecular biology and bioinformatics

Keywords: Actin, Molecular Dynamics Simulation, Actin Polymerisation, Conformational Change, Nucleotide

Corresponding Author: Mr. Thomas Splettstoesser, Dipl. Biol.

Corresponding Author's Institution: University Heidelberg

First Author: Thomas Splettstoesser, Dipl. Biol.

Order of Authors: Thomas Splettstoesser, Dipl. Biol.; Frank Noé, Ph.D.; Toshiro Oda, Ph.D.; Jeremy Smith, Prof.

Manuscript Region of Origin:

Abstract: The assembly of monomeric G-actin into filamentous F-actin is nucleotide dependent: ATP-G-actin is favoured for filament growth at the 'barbed end' of F-actin, while ADP-G-actin tends to dissociate from the 'pointed end'. Structural differences between ATP- and ADP-G-actin are examined here using multiple molecular dynamics simulations. The 'open' and 'closed' conformational states of G-actin in aqueous solution are characterised, with either ATP or ADP in the nucleotide binding pocket. With both ATP and ADP bound the open state closes in the absence of actin-bound profilin. The position of the nucleotide in the protein is found to be correlated with the degree of opening of the active site cleft. Further, the simulations reveal the existence of a structurally well-defined, compact, 'superclosed' state of ATP-G-actin, as yet unseen crystallographically and absent in the ADP-G-actin simulations. The superclosed state resembles structurally the actin monomer in filament models derived from fibre diffraction, and is putatively the polymerisation competent conformation of ATP-G-actin.

Ruprecht-Karls-Universität Heidelberg

Interdisziplinäres Zentrum für Wissenschaftliches Rechnen

Computational Molecular Biophysics

Prof. Dr. Jeremy C. Smith

Universität Heidelberg • IWR • Im Neuenheimer Feld 368 • 69120 Heidelberg

Im Neuenheimer Feld 368
D-69120 Heidelberg

Telefon +49 (6221) 54-8857
Telefax +49 (6221) 54-8868
e-mail biocomputing@iwr.uni-heidelberg.de

03. July 2008

David A. Case, *Journal of Molecular Biology*
600 Technology Square, 5th floor
Cambridge, Massachusetts 02139
USA

Dear Editor,

Please find enclosed the manuscript entitled "Nucleotide-dependence of G-actin conformation from multiple molecular dynamics simulations and observation of a putatively polymerisation-competent superclosed state", by Thomas Splettstoesser, Frank Noé, Toshiro Oda and Jeremy C. Smith, for submission as a regular research paper to the *Journal of Molecular Biology*.

The manuscript addresses the nucleotide-induced conformational transition in monomeric actin (G-actin). This transition represents a key element of the dynamic assembly and disassembly of actin filaments. Despite the abundance of ADP- and ATP-bound crystallographic structures of G-actin, the structural differences between the two states are still intensely debated. In this study we characterise ADP- and ATP-bound actin monomers with molecular dynamics simulation and report a new conformational state of ATP-G-actin. The observation of this new state in several independent simulations and its structural similarities to monomers of recent F-actin models suggest it to be the putative polymerisation-competent form of ATP-G-actin and is in agreement with previous experimental studies suggesting the existence of a polymerisation-inducing state of ATP-G-actin.

The present work makes a novel contribution to understanding of nucleotide-induced conformational changes in G-actin. As such the work will be of particular interest to the readers of the *Journal of Molecular Biology*.

Corresponding Authors:

Thomas Splettstoesser
Computational Molecular Biophysics,
Interdisciplinary Center for Computational Science (IWR),
University of Heidelberg,
Im Neuenheimer Feld 368, 69120 Heidelberg, Germany
Tel: +496221 54 8806
Fax: +496221 54 8868
E-mail: Thomas.Splettstoesser@iwr.uni-heidelberg.de

Editor
David A. Case

The following scientists are qualified to review the manuscript:

Prof. Dr. Kenneth C. Holmes
Max Planck Institute for Medical Research
Emeritus Group Biophysics
Jahnstrasse 29
69120 Heidelberg, Germany
Tel. +49 (0)6221 486270
E-mail: Ken.Holmes@mpimf-heidelberg.mpg.de

Prof. Dr. Krzysztof Kuczera
University of Kansas
Department of Chemistry
1251 Wescoe Hall Dr., Room 2010 Malott Hall
Lawrence, KS 66045-7582, USA
Tel. +1 785 864 5060
Fax. +1 785 864 5396
E-mail: kkuczera@ku.edu

Prof. Dr. Martin Zacharias
School of Engineering and Science
Bioinformatics and Computational Biology
Campus Ring 1
28759 Bremen, Germany
Tel. +49 (0)421 200 3541
Fax. +49 (0)421 200 3249
E-Mail: m.zacharias@jacobs-university.de

Dr. Steven Hayward
School of Computing Sciences and School of Biological Sciences,
University of East Anglia,
Norwich, NR4 7JT, United Kingdom
Tel: +44 (0)1603 593542
Fax: +44 (0)1603 593345

E-mail: sjh@cmp.uea.ac.uk

Prod. Dr. Klaus Schulten
3147 Beckman Institute
University of Illinois
405 N. Mathews
Urbana, IL 61801
Tel: +1 217-244 1604
Fax: +1 217 333 2922
E-mail: kschulte@ks.uiuc.edu

Prof. Dr. David D. Thomas
Department of Biochemistry, Molecular Biology, and Biophysics
University of Minnesota
6-155 Jackson Hall
321 Church St SE
Minneapolis, MN 55455, USA
Tel: +1 612 626-3322
Fax: +1 612 624 0632
E-mail: ddt@umn.edu

Due to conflict of interest we would like to exclude the following people from the editorial and review process: Dr. David Sept, Prof. Dr. Gregory A. Voth.

We hope the manuscript will be suitable for publication.

Yours sincerely,

Prof. J.C. Smith
Chair, Computational Molecular Biophysics.

Nucleotide-dependence of G-actin conformation from multiple molecular dynamics simulations and observation of a putatively polymerisation-competent superclosed state

Thomas Splettstoesser[*¶], Frank Noé[*†], Toshiro Oda[‡], Jeremy C. Smith[*§]

[*]Interdisciplinary Center for Scientific Computing, University of Heidelberg, Im Neuenheimer Feld 368, 69120 Heidelberg, Germany.
[†]DFG Research Center Matheon, FU Berlin, Arnimallee 6, 14159 Berlin, Germany.
[‡]RIKEN Harima Institute, RIKEN Spring-8 Center, 1-1-1 Kouto, Sayo, Hyogo 679-5148 Japan
[§]University of Tennessee/Oak Ridge National Laboratory, Center for Molecular Biophysics, One Bethel Valley Road, Oak Ridge, TN 37831, USA.
[¶]Correspondence: thomas.splettstoesser@iwr.uni-heidelberg.de

Short Running Title

Nucleotide-dependence of G-actin conformation

Keywords

Actin, Molecular Dynamics Simulation, Actin Polymerisation, Conformational Change, Nucleotide

Contact

Thomas Splettstoesser
IWR Heidelberg
Im Neuenheimer Feld 368
69120 Heidelberg
Tel. +49-6221-548806
Email: thomas.splettstoesser@iwr.uni-heidelberg.de

Summary

The assembly of monomeric G-actin into filamentous F-actin is nucleotide dependent: ATP-G-actin is favoured for filament growth at the ‘barbed end’ of F-actin, while ADP-G-actin tends to dissociate from the ‘pointed end’. Structural differences between ATP- and ADP-G-actin are examined here using multiple molecular dynamics simulations. The ‘open’ and ‘closed’ conformational states of G-actin in aqueous solution are characterised, with either ATP or ADP in the nucleotide binding pocket. With both ATP and ADP bound the open state closes in the absence of actin-bound profilin. The position of the nucleotide in the protein is found to be correlated with the degree of opening of the active site cleft. Further, the simulations reveal the existence of a structurally well-defined, compact, ‘superclosed’ state of ATP-G-actin, as yet unseen crystallographically and absent in the ADP-G-actin simulations. The superclosed state resembles structurally the actin monomer in filament models derived from fibre diffraction, and is putatively the polymerisation competent conformation of ATP-G-actin.

Introduction

Actin is a structural protein of eukaryotes that has several key roles in the functioning of the cell (1, 2). As a major component of the cytoskeleton, actin is responsible for the shape and structural integrity of the cell. The motility of migrating cells is based on continuous rearrangements of the actin cytoskeleton. Several classes of the motor protein myosin transport vesicles along actin filaments across the cell and in muscle, actin interacts with myosin to cause contraction.

Two forms of actin exist: globular monomers (G-actin) and asymmetric filamentous polymers (F-actin), the latter being the biologically active form of actin. The G-actin molecule consists of four subdomains which form a nucleotide binding site in the centre of the protein (1). ATP-bound G-actin polymerises helically to form two-stranded F-actin filaments (2) exhibiting molecular polarity based on the head-to-tail orientation of the subunits, with a growing 'barbed' end and a trailing 'pointed' end. This polarity determines the mechanism of actin assembly in cells. Filament growth is favoured at the barbed end where ATP-G-actin assembles to the filament. Following polymerisation, ATP is hydrolysed within the fibril. The slow release of inorganic phosphate then triggers a conformational change in the filament, leading to a significant increase of the filament's flexibility (3) and promoting its disassembly at the pointed end. The dissociated ADP-G-actin monomers are subject to nucleotide exchange, often mediated by the actin-binding protein profilin (4). The resulting ATP-G-actin is polymerisation competent whereas the low affinity of ADP-G-actin with the filament prevents its assembly to F-actin *in vivo*. Thus, it is the nucleotide that drives the actin cycle of assembly and disassembly and regulates the equilibrium between G and F-actin. ADP and ATP-F-actin differ not only in

terms of flexibility but the two forms also serve as a timer for the cell to distinguish between older and newer stretches of the filament (5).

Although actin is a well-studied protein, the underlying mechanism of its dynamic behaviour is not well understood. There are no X-ray crystallographic structures of the filament, but several models, derived from low-resolution data, have been proposed (8, 9). More recent contributions include the 2004 Holmes model (6) and the 2008 Oda model (7).

Fundamental questions exist also regarding the monomer. Because the critical concentration of ATP-G-actin for assembly to the barbed end of the filament is much lower than that of the ADP form, there is believed to be a nucleotide-induced conformational switch in the protein. However, although more than 40 X-ray crystallographic structures of G-actin have been solved, both in the ATP- (12, 13) and ADP-bound (8) states, the nature of the conformational difference between the two states remains unclear and is the subject of ongoing debate (15, 16).

In all but one of the reported crystal structures the cleft between the two lobes of actin, subdomains 2 and 4, is closed. However, in the structure of Ref. (9), (Protein Data Bank (PDB) (10) code 1HLU), the interdomain distance is significantly larger and the structure thus more open. This 'open state' of actin has been hypothesised to represent the ADP-state of monomeric actin (19, 20), while the 'closed state' may correspond to the ATP form (Fig. 1). Furthermore, electron microscopic studies of yeast actin filaments showed that the cleft between subdomain 2 and 4 is open in ADP-filaments but closes when those filaments are incubated with the γ-phosphate analogue BeF_3^-, thus supporting the 'open' and 'closed' state hypothesis (11). However, this hypothesis has been challenged (13, 14)

and a competing model suggests a nucleotide-dependent conformational change in the DNase I binding loop of subdomain 2 (residues 40-51) to be responsible for the functional difference (8). According to this model the DNase binding loop is disordered in the ATP state but folds into an α–helix in the ADP state. Unlike most other crystal structures reported, the recent structures of ATP and ADP-G-actin in Ref. (12) were free of co-crystallised proteins or attached chemical compounds. Apart from the γ-phosphate sensor loop the two structures are strikingly similar and appear to support neither of the above hypotheses.

The nucleotide dependence of the G-actin structure has also been examined by molecular dynamics simulation (MD). In a study of the open *vs.* closed model, it was found that in the open state of actin, the nucleotide-binding pocket of ATP-G-actin closes in absence of the co-crystallised profilin but remains open if profilin is present (13). No significant structural changes were observed in the simulations of the closed state. However, only one simulation of one ns was conducted for each of the ATP and ADP states, precluding a statistically significant assessment of the relationship between nucleotide state and monomer structure. In a very recent study, MD simulations were conducted of G-actin in the closed state (14). It was concluded that the nucleotide binding cleft is closed regardless of the nucleotide binding state. In addition, no correlation of the conformation of the DNase I binding loop with either ADP or ATP binding was found. In contrast to Ref. (14), the conformation of the DNase binding loop was observed to be nucleotide dependent in the molecular dynamics study of Ref. (15). In Ref. (15), again single simulations were performed on closed-state structures based on PDB ID 1J6Z and 1NWK, and the helical DNase binding loop was seen to unfold in the ATP state but

remains stable in the ADP state over a time span of 50 ns. In summary, the nucleotide-mediated changes in G-actin conformation remain the subject of debate.

The aim of the present work is similar to that of Refs. (22, 23, 24) above, *i.e.*, to use MD simulation to shed light on the nucleotide-induced conformational changes in G-actin that allow the ATP-bound form to polymerise but prevent ADP-bound actin from doing so. However, here a large number of multiple nanosecond-timescale MD simulations of open- and closed-state actin are performed, with a total simulation time of 440 ns. As a result, some observations are found to be statistically significant. Both the open state (9) and the closed state (16) structures used were co-crystallised with profilin and the bound nucleotide, ATP. For the formation of the open-state crystals, a salt molarity of 1.8 M KPO_4 appears to be crucial. When the molarity was changed from 1.8 M to 3.6 M, the dimensions of the unit cell decreased to that of a closed state crystal, raising doubt about the stability of the open state structure outside the crystal lattice (17). Therefore, to examine whether the open state is also stable in absence of profilin, MD simulations were carried out with and without profilin. For comparison, structures of the closed state of actin were also simulated.

To further investigate the effects of the nucleotide on the actin structure unbiased by profilin, additional simulations were performed using other X-ray structures of higher resolution (12). All simulations were carried out both with ATP and ADP in the nucleotide-binding pocket.

Results

Open-state G-actin molecular dynamics simulations were performed to investigate the stability of the open domain cleft and the effects on it of the binding of ATP, ADP and profilin. Furthermore, ATP and ADP-actin were studied in the closed state. For each state studied at least 10 simulations of 4 ns were performed, from different distributions of starting velocities, in order to determine the statistical significance of the phenomena observed.

Cleft Size and its Relation to the Nucleotide Position

The cleft size is a measure of how 'open' or 'closed' a G-actin structure is, and is defined (18) as the distance between the centers of mass of the protein backbone of residues 57-69, and 30-33 in subdomain 2 and residues 203-216 in subdomain 4. In Fig. 4 are shown time series of this domain cleft size. Each line in the figure is an average over 10 MD simulations for the open state results and over 20 simulations for the ATP and ADP closed states.

In the open state crystal structure (1HLU) the cleft size is 21.1 Å whereas it is 16.7 Å in the closed state crystal structure (2BTF). All average MD domain cleft distances stabilise after 100-1000 ps. The profilin-bound open-state simulations (with either ATP or ADP bound) remain the most widely open, with an average cleft size of ~20.5 Å, close to that of the starting structure (21.1 Å). The profilin-bound actin cleft is ~4 Å wider than the closed state MD systems and 1-2 Å wider than the corresponding open state simulations without profilin.

The removal of profilin is accompanied by a significant partial closing of the cleft, visible in Fig. 4 as a sharp decrease in the interdomain distance over the first ~300 ps of the simulation sets concerned. The two simulation sets of the closed state, again with ATP and ADP, exhibit stable domain distances close to their starting value of 16.7 Å and approximately 3 Å narrower than the corresponding simulations of the open state. Finally, Fig. 4 also shows that, for the simulations in the absence of profilin, the ADP-bound structures are slightly, but significantly, wider open than those with ATP.

In Fig. 5 the same data as in Fig. 4 are shown as time-averaged probability densities of the cleft size. In the two open-state simulation sets with bound profilin the density has slightly shifted from the open-state starting point towards the closed state. However, this shift is much more prominent in the two open-state simulations without profilin, and the main peak of both open-state non-profilin simulations is closer to that of the crystal structure of the closed than the open state. In the two closed-state simulation sets the cleft size probability maximum remains close to the starting value.

Graphical inspection of the MD trajectories and comparison with the open and closed starting structures (Fig. 2) showed significant variations in the nucleotide position. In the closed-state X-ray structure the nucleotide is located in its binding pocket, stabilised by multiple hydrogen bonds. In contrast, in the open state the nucleotide is less deeply buried, wedged between its two binding loops, with many of the stabilising interactions present in the closed state disrupted. In the majority of open-state trajectories in which the nucleotide relocated into the binding pocket, an accompanying closure of the domain cleft was observed. However, in some open-state simulations the nucleotide remained in its position or moved out of the binding site even further, and in these simulations the

cleft tended to remain open, with larger cleft-size fluctuations. This tendency is more prominent in the simulations of the open state with ADP, explaining the larger average cleft size in the ADP rather than ATP state.

The depth of the nucleotide in the binding pocket was calculated (see 'Methods') for each simulation frame and its correlation with the corresponding interdomain cleft size computed. For simulations without profilin, the average correlation coefficient between nucleotide depth and cleft size is 0.64. Thus, the cleft size is clearly related to the position of the nucleotide in the binding pocket.

The hydrogen bonding pattern between the protein and the nucleotide is dependent on the cleft size (Fig. 7). In the ATP-bound closed and open state simulations (without profilin), structures with a closed domain cleft possess an average number of nucleotide:protein hydrogen bonds of 10 to 12. In contrast, the average number of hydrogen bonds decreases with an increasing cleft size, becoming <7 for the most open structures. The averages of the ADP simulations are generally lower, owing to the missing phosphate group. However, due to the poor stabilisation of the ADP in the initial open state structure, the corresponding simulations show less variation with cleft size of the H-bond occupancy and over a larger range of cleft sizes than the other simulations.

In Fig.7, even at cleft sizes around the range of the closed state, the open state simulations with ADP show a much lower number of hydrogen bonds than their closed-state counterparts. This difference suggests that the cleft size parameter alone may not be a good indicator of whether a MD structure has adopted the overall conformation of the closed state as found in crystal structures: open-state ADP simulations that exhibit small cleft sizes may not have necessarily reached the closed state.

The Superclosed State

Examination of the cleft size probability density in Fig. 5 shows a close similarity between the ATP and ADP closed state simulation sets. In both cases the main peak is at ~16 Å, close to the initial value of those simulations, 16.7 Å. However, in the closed ATP simulations there is a second, smaller peak in the distribution at ~13.7 Å. This additional state of ATP-G-actin possesses a cleft size ~3 Å smaller than that of the closed state and we therefore label it the 'superclosed state'. This state was strongly populated in four out of the 20 closed ATP simulations but never populated in the corresponding ADP simulations.

Fig. 6 shows time series of the cleft size for the four superclosed-state simulations. In each of these simulations the superclosed state is seen to persist for several nanoseconds. Apart from the similar cleft sizes, the structures of the four superclosed-state trajectories also show other very similar structural features.

To further characterise the superclosed state, a representative superclosed-state structure was taken as a starting structure to perform additional MD simulations (see 'Methods'). Twenty short (1 ns) simulations were performed with this superclosed ATP-actin as the starting structure and another 20 simulations in which the nucleotide γ–phosphate group was removed so as to replace ATP by ADP. In 6 of the 20 simulations of superclosed ADP-actin the protein structure left the superclosed state within the relatively short 1 ns of simulation time. In contrast, only 2 of the 20 ATP-bound actin simulations left the superclosed state, confirming that ATP stabilises the superclosed state.

Two sets of simulations (with ADP and with ATP) were also performed starting from closed-state structures crystallised in the absence of profilin (1.8 Å resolution structures of free ADP- and ATP-bound actin in Ref. (12)). 10 simulations of 4 ns were carried out each. In agreement with the previous simulations, ATP-G-actin occupies both the closed and superclosed states while the ADP-bound form adopts the closed state.

Structural Features of the Superclosed State

The increased cleft closure in the superclosed state is achieved by rotations of subdomains 2 and 4 (Fig. 8). Relative to the closed state starting structure, in the average superclosed state structure, subdomains 2 and 4 are rotated by about 8° and 13°, respectively. These rotations remove the steric hindrance between the subdomains that would prevent the closed state from further closing its cleft.

A comparison of the superclosed structure with that of recent filament models by Holmes and Oda revealed similar orientations of subdomains 2 and 4. For example, in Fig. 8C are shown the superclosed state and a monomer taken from the Oda filament model, both aligned to the structure of the closed state. The arrows in the figure indicate the similar subdomain orientations of superclosed state and the Oda model, which are clearly different from the structure of the closed state. Furthermore, the cleft distances of 15 Å in the Holmes model and 13.1 Å in Oda's model are similar to that of the average superclosed state (13.7 Å).

Also of interest is the propeller angle, defined by the dihedral angle of the centres of masses of the four subdomains. The average propeller angle of G-actin (Fig. 9) converged to about 16.3° in all but the open ADP simulations for which the mean is

19.8°±0.75. However, the average of the four superclosed trajectory segments is 10.7±1.77°, much smaller than the average closed-ATP-simulation propeller angle Similar results were observed in the simulations performed starting from structures crystallised in the absence of profilin (PDB ID 2HF3 and 2HF4) - the average propeller angles of these ADP- and ATP-states were found to be 20.6±0.79° and 16.5±0.79°, whereas the average superclosed-state propeller angle is 10.5±2.13°. In comparison, the propeller angles of the Holmes and Oda filament models are 3.6° and 5°, respectively. Thus, also with respect to the propeller angle, the superclosed state is the G-actin conformation that is most similar to the filament models.

Structure of the DNase I Binding Loop

Finally, to examine the possibility of a nucleotide-mediated conformational change in the DNase binding loop, an analysis was performed of the secondary structure of the binding loop in the present simulations using the DSSP tool (19). In both of the present starting conformations the loop is disordered. During all simulations the α–helical fold occurred very rarely in the DNase binding loop and was short lived - in the 80 ns of closed-state ATP simulation the DNase binding loop adopted an α–helical conformation only 0.011% of the simulation time, this percentage being 0.114% in the corresponding closed-state ADP simulations. In the open state simulations, the α–helical fold was similarly rare. Therefore, there is no evidence from the present simulations for a coupling between the nucleotide-binding state and the conformation of the DNase I binding loop.

Discussion

The present simulations indicate that the open state of G-actin is unstable in absence of profilin, in agreement with a previous single-trajectory MD study (13). The correlation of the nucleotide depth with the cleft size suggests that the instability is based on the initial position of the open-state nucleotide which is located partially out of the binding pocket and poorly stabilised *i.e.* with few hydrogen bonds. In contrast, the open conformation of actin remains relatively stable when bound to profilin. Occasional, short-lived opening of the cleft to the extent of the open state structure was observed in only 4 out of the 40 simulations of the closed state. Thus, the profilin-bound, open-state crystal structure (1HLU) may represent a stable actin-profilin-complex in which actin is opened to facilitate nucleotide exchange, but is unlikely to represent a stable conformation of the isolated actin monomer. Further, the instability of the open state suggests that this state is not responsible for the different polymerisation rates of ATP and ADP-G-actin.

A clear correlation is found between the cleft size and the position of the nucleotide. In crystal structure of the open state PDB 1HLU the ATP is wedged between two lateral nucleotide binding loops, which are located at the base of subdomains 2 and 4, respectively. Keeping the loops apart prevents actin from adopting a closed state. The nucleotide position variations do not converge in the simulations. Consequently, in simulations where the nucleotide phosphate groups remained partly outside the pocket or the nucleotide slipped further out, the protein was left in a more highly fluctuating open conformation. In simulations in which the nucleotide fully entered the binding pocket and where its position is stabilised, full closure of the cleft was observed. The absence of convergence in nucleotide position/cleft size resulted in a stable closure of the cleft being

observed only in half of the open state simulations without profilin, and this explains why the average cleft sizes of simulations with ATP bound starting from the crystal structures of the open and closed states did not converge.

Of all the simulations performed, those of the open-state ADP-bound actin without profilin exhibited the largest range of cleft sizes (15 to 26 Å), the lowest average number of nucleotide:protein hydrogen bonds (Fig. 7) and the largest propeller angle (Fig. 9). This may be due to the starting structure being far from native, as it was taken from a crystal structure in which both the profilin and the γ-phosphate group were removed, leaving the ADP in a solvent exposed, poorly hydrogen-bonded position. The resulting lack of nucleotide stabilisation leads to highly fluctuating behaviour.

In general the average number of hydrogen bonds to the nucleotide is high at smaller cleft sizes and low at larger cleft sizes. This correlation does not depend on the nucleotide or whether the simulation was started with an open or a closed actin conformation. This may be an indication that the closed state, as found in most X-ray studies, is favourable because the nucleotide holds together the two domains of actin - nucleotide-free G-actin has been shown to denature rapidly in absence of stabilising agents (20). With an increased number of nucleotide:protein hydrogen bonds the protein adopts a more compact state.

The conformation of the DNase binding loop was observed to be nucleotide dependent in the single 50 ns molecular dynamics study of α-actin in Ref. (15). In the present study on β-actin (sequence identity with α-actin of >90%), using 140 simulations for a total simulation time of 440 ns, no indication was found of a nucleotide dependence of the DNase I binding loop conformation. This is also in agreement with a previous single 5 ns

simulation study of Ref. (14). In the present work very few, short-lived (<500 ps) instances occurred of the DNase binding loop adopting an α-helix fold. The results therefore provide no evidence for a nucleotide-induced change to the α-helix conformation.

The present MD simulations of G-actin reveal a new distinct state, found exclusively in closed ATP –bound actin, that is more compact than the regular closed state and is thus referred to as 'superclosed'. In comparison to a typical closed state structure (e.g. 2BTF), in the superclosed state subdomains 2 and 4 have a different relative orientation, thus allowing the cleft to be completely closed. The possibility exists that the newly-observed superclosed state of ATP-G-actin may be the polymerisation-competent conformation that is required for filament assembly. The superclosed structure displays striking similarities with proposed low-resolution filament models derived from experiment. The same orientation of the two subdomains, complete cleft closure and similar propeller angles are also present in actin filament models. This well-defined superclosed state was observed in several independent ATP-actin simulations, indicating its statistical relevance. Furthermore, formation of the superclosed state was observed in ATP-actin simulations of different PDB starting structures (2BTF and 2HF4).

The increased compactness of the superclosed state may be a requirement for polymerisation. Furthermore this state occurs only in ATP-G-actin simulations of the closed state but in none of the ADP-simulations. This is consistent with the behaviour of actin *in vivo*, where only ATP-G-actin assembles to F-actin but not the ADP-bound form. Our findings are in agreement with experimental proteolysis (21) and spectroscopy studies (22) where ATP-G-actin was found to undergo conformational changes leading to

a ‘F-actin-monomer’ (or ‘G*-actin’) form which favours polymerisation. This proposed form of ATP-G-actin showed characteristics of both G- and F-actin and may correspond to the superclosed state of actin described in this study.

Why hasn’t a superclosed structure been observed crystallographically? The crystallisation of actin has always been a challenge, as at high concentrations G-actin tends to polymerise to F-actin rather than to crystallise. Because of this problem, G-actin has been co-crystallised with an actin-binding protein (12, 17), chemically modified (8), mutated (12) or otherwise rendered non-polymerisable (23). These alterations, possibly together with the non-physiological conditions of the crystalline state, might prevent formation of the superclosed state.

Although the present superclosed state is a putative candidate for the *polymerisation-competent* form of G-actin, the closed state may still be the predominant state of ATP-G-actin in equilibrium and therefore much more likely to be observed experimentally. Further experimental studies on actin are required to confirm or otherwise whether the superclosed state is that involved in G-actin polymerisation. Because of the similarities with actin monomers of present medium-resolution filament models, the superclosed structure might prove useful for interpreting to fibre diffraction data or electron micrographs of F-actin so as to derive improved models in the future.

Methods

Simulation Models

A summary of the simulation models and the system sizes is given in Table 1. The first set of simulations investigates the stability of the open state as a function of nucleotide and profilin binding. The only existing X-ray structure of G-actin with an open cleft, PDB ID 1HLU (9), was used to model the open state. The co-crystallised profilin was included in one set of simulations and removed in a further set.

Closed state simulations were conducted based on two PDB structures:

1) PDB ID 2BTF (16), chosen because the amino-acid sequence is identical with that of the 1HLU structure, used in the open-state simulations. The profilin coordinates were removed.

2) To examine whether the results of closed state simulations based on PDB 2BTF also hold for other PDB structures, simulations were also performed on PDB ID 2HF3 for the ADP-state and 2HF4 for the ATP-state (12). Unlike 1HLU and 2BTF, 2HF3 and 2HF4 are from *Drosophila melanogaster* and are unbiased by co-crystallised proteins or attached molecules. Instead, actin was rendered unpolymerisable by introducing two point mutations. Here, these mutations were reverted so as to simulate actin in its native form.

The three ADP-bound actin simulations based on 1HLU (with and without profilin) and 2BTF were set up in the same way as those described above but the γ–phosphate group was removed from the nucleotide and replaced by two water molecules.

The protonation states of the histidine residues were derived by calculating pK values using the H++ webserver (24), resulting in double protonation of both His^{88} and His^{101}.

In the actin crystal structures used, His^{73} is methylated. This methylation has been shown experimentally to be a major determinant of stability and conformational flexibility of the actin monomer (25). Hence, a patch was applied to His^{73} to remove the relevant hydrogen atom and replace it with the methyl group, using standard CHARMM parameters. The proteins were solvated with 12 Å of water, resulting in cubic boxes of 91 Å side length for the simulations without profilin and 104 Å for the simulations of profilin-bound actin. Overlapping water molecules within 1.4 Å of the protein were deleted. Physiological concentrations of 139 mM K^+, 12 mM Na^+ and 16 mM Cl^- were used, mimicking cytosolic conditions, and the number of Cl^- ions was adjusted to neutralise the actin systems. In the crystallographic structures calcium or strontium ions are present in the nucleotide binding pocket. These were replaced by a magnesium ion, again to reflect *in vivo* conditions (26).

A further set of simulations was performed, using two models aimed at determining the stability of a newly-found 'superclosed' state, described below, as a function of the bound nucleotide. Since the superclosed state has a cleft size of around 13.7 Å, the starting structure for these simulations was chosen as the lowest-potential energy structure from all closed-ATP-simulation structures with cleft sizes in the range 13.6 to 13.8 Å. For the simulations of the superclosed state with ADP in the nucleotide binding

pocket, the γ–phosphate group of ATP was removed and the number of counter ions adjusted to neutralise the system.

Molecular Dynamics Simulations

The initial structures were prepared using the CHARMM 31b2 software (27) and molecular dynamics simulations were carried out with the NAMD package , 35applying the CHARMM22 force field (28). The TIP3P water model (29) was used. The SHAKE algorithm (30) was employed to constrain all bonds involving hydrogen atoms, which allowed a 2 fs time step. A smooth switching function at 8 Å and a cutoff of 10 Å was applied for short-range electrostatics and van der Waals interactions. For long-range electrostatic interactions, which were calculated every 4 fs, the Particle Mesh Ewald method (31) with a nonbonded cutoff of 10 Å was used.

The systems were minimised using the conjugate gradient algorithm for 5000 steps with the protein and nucleotide atoms harmonically constrained. The MD simulations were performed using the leap-frog integrator in the isothermal-isobaric ensemble (NPT) at 1 atm pressure, with periodic boundary conditions applied. The Nosé-Hoover Langevin piston (32) with a decay period of 500 fs was employed. The systems were gradually heated to 300 K with the harmonic constraints still in place. The constraints were gradually lifted (0.5, 0.25, 0.05 kcal/mol) during the three subsequent equilibration steps of 25 ps length each. After the heating and equilibration period 4 ns of production run were carried out for each simulation.

Observables

Nucleotide Depth

The nucleotide phosphate groups may be buried to various extents in the nucleotide binding cleft. In this regard the open and closed X-ray structures differ greatly: in the closed state, the nucleotide is positioned deep in the binding pocket, while in the open structure it is almost outside the pocket (Fig. 2).

Determination of the relative nucleotide position in the MD trajectories is non-trivial because of the flexible topology of the binding pocket. The following procedure was adopted. The crystallographic open and closed structures were superimposed using least-squares alignment and a 'depth vector' defined, connecting the positions of the two β-phosphate atoms. The structure of every MD frame was then least-squares aligned with the open-state structure. For a given trajectory frame the nucleotide depth is defined as the distance between the projection of the β-phosphate onto the depth vector and the position of the open state β-phosphate (Fig. 3). A nucleotide depth value of zero corresponds to the open state nucleotide depth and a value of 3.3 Å to that of the closed state.

Propeller Angle

G-actin consists of four subdomains which form a U-shaped structure. The dihedral angle between the centres of mass of the four subdomains (excluding the very flexible DNase I binding loop, Arg^{39}-Lys^{50}, and the 'hydrophobic plug', Gln^{263}-Ser^{271}) is referred to here as the propeller angle. A schematic depiction can be found in Fig. 9. An angle of 0°

corresponds to the most planar structure of the protein. For the calculation of the average propeller angles the first nanosecond of each production run was ignored.

Subdomain Rotation

The program DynDom Domain Select (33) determines axes and degrees of rotation of domains between two structures. For this calculation, subdomains 1 and 3 of the two structures were aligned with an RMSD fit and the rigid-body movements of subdomains 2 and 4 were then determined using DynDom.

All molecular images were produced with the molecular graphics program PyMol (DeLano 2002).

Acknowledgements

We thank Prof. Kenneth Holmes for providing us with his F-actin model. This work was supported in part by the Baden-Württemberg, Forschungsschwerpunktprogramm "Biomimetische Modelle der Zellmechanik", grant number 24-7532.22-19-12/1. The majority of the computations were performed on the HeLiCs supercomputer (http://helics.unihd.de) at the Interdisziplinäres Zentrum für Wissenschaftliches Rechnen (IWR) in Heidelberg.

References

1. Kabsch, W., Mannherz, H.G., Suck, D., Pai, E.F. and Holmes, K.C. (1990). Atomic structure of the actin: DNase I complex. Nature. 347, 37-44.

2. Small, J.V., Isenberg, G. and Celis, J.E. (1978). Polarity of actin at the leading edge of cultured cells. Nature. 272, 638-639.

3. Isambert, H., Venier, P., Maggs, A.C., Fattoum, A., Kassab, R., Pantaloni, D. and Carlier, M.F. (1995). Flexibility of actin filaments derived from thermal fluctuations. Effect of bound nucleotide, phalloidin, and muscle regulatory proteins. J. Biol. Chem. 270, 11437-11444.

4. Perelroizen, I., Didry, D., Christensen, H., Chua, N.H. and Carlier, M.F. (1996). Role of nucleotide exchange and hydrolysis in the function of profilin in action assembly. J. Biol. Chem. 271, 12302-12309.

5. Pollard, T.D., Blanchoin, L. and Mullins, R.D. (2000). Molecular mechanisms controlling actin filament dynamics in nonmuscle cells. Annu. Rev. Biophys. Biomol. Struct. 29, 545-576.

6. Holmes, K.C., Schröder, R.R., Sweeney, H.L. and Houdusse, A. (2004). The structure of the rigor complex and its implications for the power stroke. Philos. Trans. R. Soc. Lond. B. Biol. Sci. 359, 1819-1828.

7. Oda, T., Stegmann, H., Schröder, R.R., Namba, K. and Maéda, Y. (2007). Modeling of the F-actin structure. Adv. Exp. Med. Biol. 592, 385-401.

8. Otterbein, L.R., Graceffa, P. and Dominguez, R. (2001). The crystal structure of uncomplexed actin in the ADP state. Science. 293, 708-711.

9. Chik, J.K., Lindberg, U. and Schutt, C.E. (1996). The structure of an open state of beta-actin at 2.65 A resolution. J. Mol. Biol. 263, 607-623.

10. Berman, H.M., Westbrook, J., Feng, Z., Gilliland, G., Bhat, T.N., Weissig, H., Shindyalov, I.N. and Bourne, P.E. (2000). The Protein Data Bank. Nucleic Acids Res. 28, 235-242.

11. Belmont, L.D., Orlova, A., Drubin, D.G. and Egelman, E.H. (1999). A change in actin conformation associated with filament instability after Pi release. Proc. Nat. Acad. Sci. U.S.A. 96, 29-34.

12. Rould, M.A., Wan, Q., Joel, P.B., Lowey, S. and Trybus, K.M. (2006). Crystal structures of expressed non-polymerizable monomeric actin in the ADP and ATP states. J. Biol. Chem. 281, 31909-31919.

13. Minehardt, T.J., Kollman, P.A., Cooke, R. and Pate, E. (2006). The open nucleotide pocket of the profilin/actin x-ray structure is unstable and closes in the absence of profilin. Biophys. J. 90, 2445-2449.

14. Dalhaimer, P., Pollard, T.D. and Nolen, B.J. (2008). Nucleotide-mediated conformational changes of monomeric actin and Arp3 studied by molecular dynamics simulations. J. Mol. Biol. 376, 166-183.

15. Zheng, X., Diraviyam, K. and Sept, D. (2007). Nucleotide effects on the structure and dynamics of actin. Biophys. J. 93, 1277-1283.

16. Schutt, C.E., Myslik, J.C., Rozycki, M.D., Goonesekere, N.C. and Lindberg, U. (1993). The structure of crystalline profilin-beta-actin. Nature. 365, 810-816.

17. Graceffa, P. and Dominguez, R. (2003). Crystal structure of monomeric actin in the ATP state. Structural basis of nucleotide-dependent actin dynamics. J. Biol. Chem. 278, 34172-34180.

18. Wriggers, W. and Schulten, K. (1997). Stability and dynamics of G-actin: Back-door water diffusion and behavior of a subdomain 3/4 Loop Biophys. J. 73, 624-639.

19. Kabsch, W. and Sander, C. (1983). Dictionary of protein secondary structure: pattern recognition of hydrogen-bonded and geometrical features. Biopolymers. 22, 2577-2637.

20. De La Cruz, E.M., Mandinova, A., Steinmetz, M.O., Stoffler, D., Aebi, U. and Pollard, T.D. (2000). Polymerization and structure of nucleotide-free actin filaments. J. Mol. Biol. 295, 517-526.

21. Rich, S.A. and Estes, J.E. (1976). Detection of conformational changes in actin by proteolytic digestion: evidence for a new monomeric species. J Mol Biol. 104, 777-792.

22. Rouayrenc, J.F. and Travers, F. (1981). The first step in the polymerisation of actin. Eur. J. Biochem. 116, 73-77.

23. Klenchin, V.A., Khaitlina, S.Y. and Rayment, I. (2006). Crystal structure of polymerization-competent actin. J. Mol. Biol. 362, 140-150.

24. Gordon, J.C., Myers, J.B., Folta, T., Shoja, V., Heath, L.S. and Onufriev, A. (2005). H++: a server for estimating pKas and adding missing hydrogens to macromolecules. Nucleic Acids Res. 33, W368-71.

25. Yao, X., Grade, S., Wriggers, W. and Rubenstein, P.A. (1999). His(73), often methylated, is an important structural determinant for actin. A mutagenic analysis of HIS(73) of yeast actin. J. Biol. Chem. 274, 37443-37449.

26. Estes J E, Selden L A, Kinosian H J, Gershman L C (1992). Tightly-bound divalent cation of actin J. Mus. Res & Cell Mot. 13, 272-284.

27. Brooks B.R., Bruccoleri R.E., Olafson B.D., States D.J., Swaminathan S., Karplus M. (1983). CHARMM: A program for macromolecular energy, minimization, and dynamics calculations J. Comp. Chem. 4, 187-217.

28. MacKerell, A.D., Bashford, D., Bellott, M., Dunbrack, R.L., Evanseck, J.D., Field, M.J., Fischer, S., Gao, J., Guo, H., Ha, S., Joseph-McCarthy, D., Kuchnir, L., Kuczera, K., Lau, F.T.K., Mattos, C., Michnick, S., Ngo, T., Nguyen, D.T., Prodhom, B., Reiher, W.E., Roux, B., Schlenkrich, M., Smith, J.C., Stote, R., Straub, J., Watanabe, M., Wiorkiewicz-Kuczera, J., Yin, D., and Karplus, M. (1998). All-atom empirical potential for molecular modeling and dynamics studies of proteins J. Phys. Chem. B. 102, 3586-3616.

29. Jorgensen W L, Chandrasekhar J, Madura J D, Impey R W, Klein M L (1983). Comparison of simple potential functions for simulating liquid water J. Chem. Phys. 79 (2), 926-935.

30. Ryckaert, J. and Ciccotti G, B.H. (1977). Numerical integration of the cartesian equations of motion of a system with constraints: Molecular dynamics of n-alkanes J. Comput. Phys. 23, 327-341.

31. Darden, T., York, D. and Pedersen, L. (1993). Particle mesh Ewald: an Nlog(N) method for Ewald sums in large systems J. Chem. Phys. 98, 10089-10092.

32. Evans, D. J., and B. L. Holian (1985). The Nose-Hoover thermostat. J. Chem. Phys. 83, 4069-4074.

33. Hayward, S. and Lee, R.A. (2002). Improvements in the analysis of domain motions in proteins from conformational change: DynDom version 1.50 J. Mol. Graph. 21(3), 181-183.

Figures and Tables

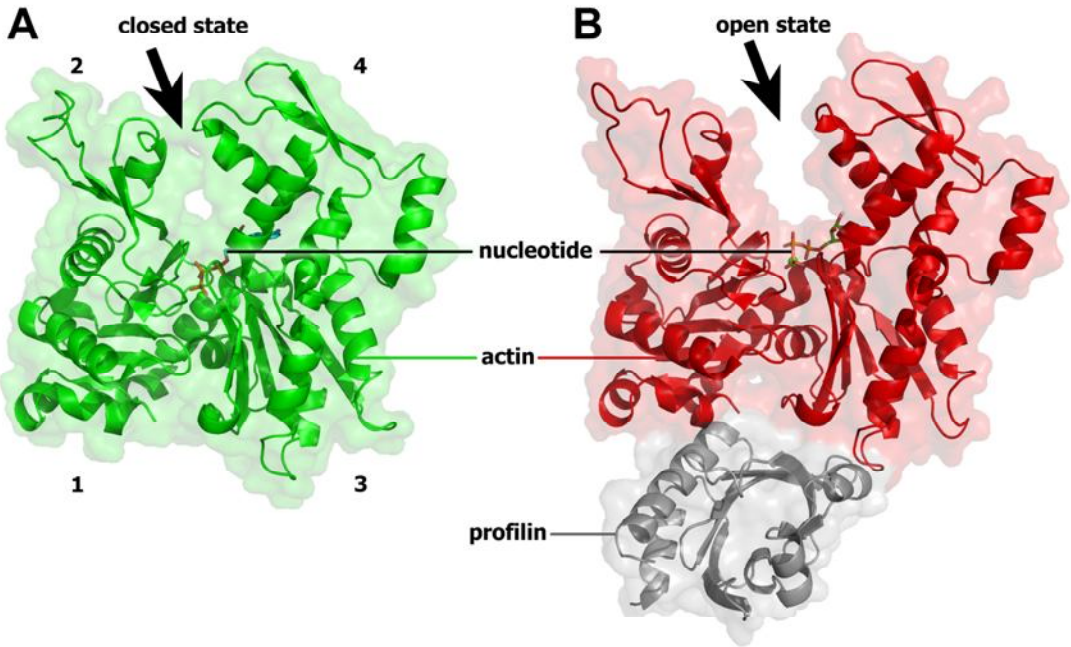

Figure 1. The closed and open states of G-actin. The nucleotide (ATP or ADP) is located in the centre of the protein. The main difference between the two structures is the size of the cleft between subdomain 2 and 4 indicated by an arrow.

A – The closed state of G-actin based on PDB ID 2BTF (11). The bound profilin is not shown. Subdomains 1-4 are labelled. The cleft between subdomain 2 and 4 is closed.

B – G-actin in the open state (PDB ID 1HLU) with bound profilin (16). The interdomain distance is considerably longer than in the closed state

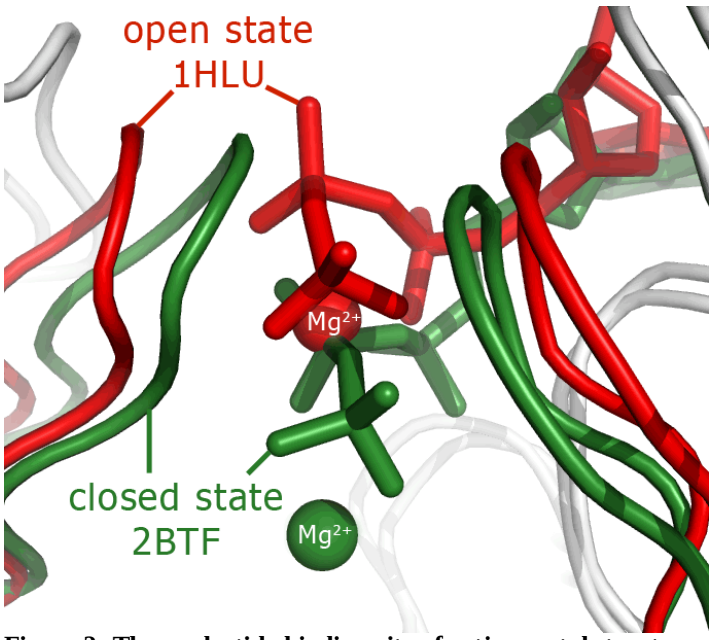

Figure 2. The nucleotide binding site of actin crystal structures. PDB 1HLU (red, open state (16)) and PDB 2BTF (green, closed state (11)). For clarity, the phosphate sensor loop is not shown. In the closed state ATP is buried in the nucleotide binding pocket with the two binding loops closed above. In contrast the ATP of the open state is located 2.8 Å away from the binding pocket, wedged between the two binding loops.

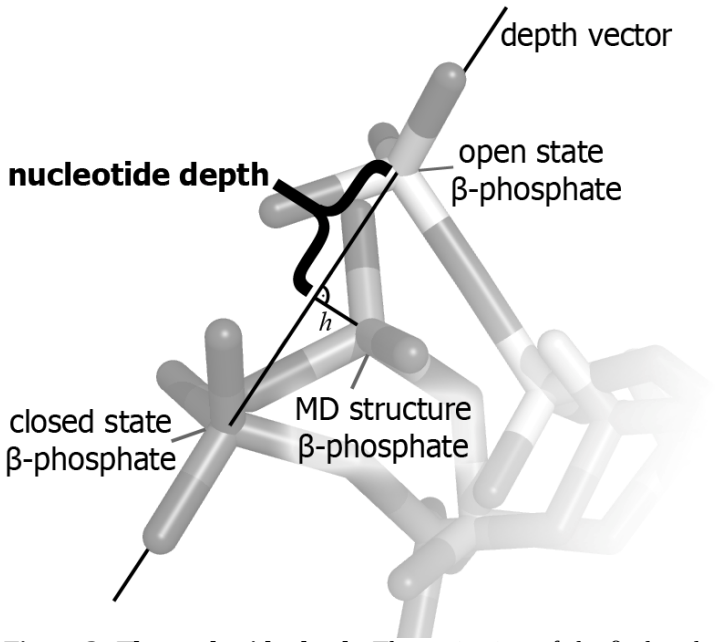

Figure 3. The nucleotide depth. The projection of the β-phosphate onto the depth vector allows the effective nucleotide depth to be calculated relative to the two states. The distance between this projection and the open state β-phosphate position is defined as nucleotide depth.

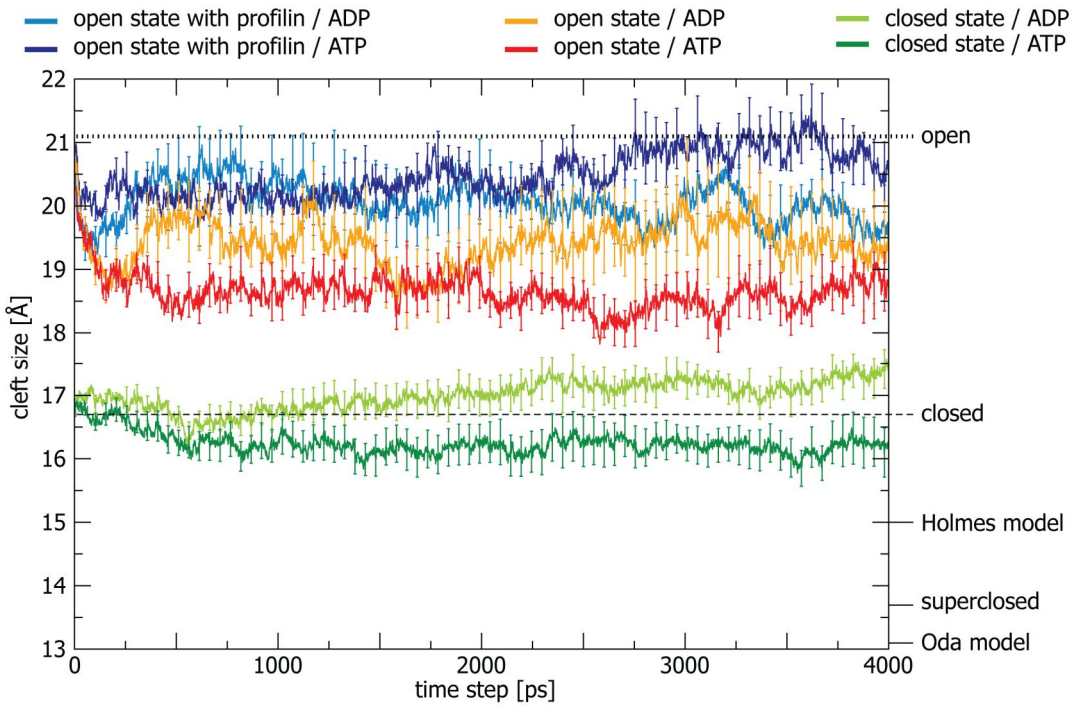

Figure 4. Time series of the average size of the cleft size during MD simulations of different states, bound nucleotide and with or without profilin. All graphs of the open state show the average over 10 MD simulation runs. The closed state graphs represent the average over 20 MD simulations each. The data are shown only for the production runs of 4 ns. The error bars correspond to one standard deviation of the mean. The black dotted line represents the domain distance of the open state and the dashed line that of the closed state starting structures.

On the right axis are marked the cleft sizes of the open and closed starting structures together with the Holmes and Oda filament models and the average superclosed state

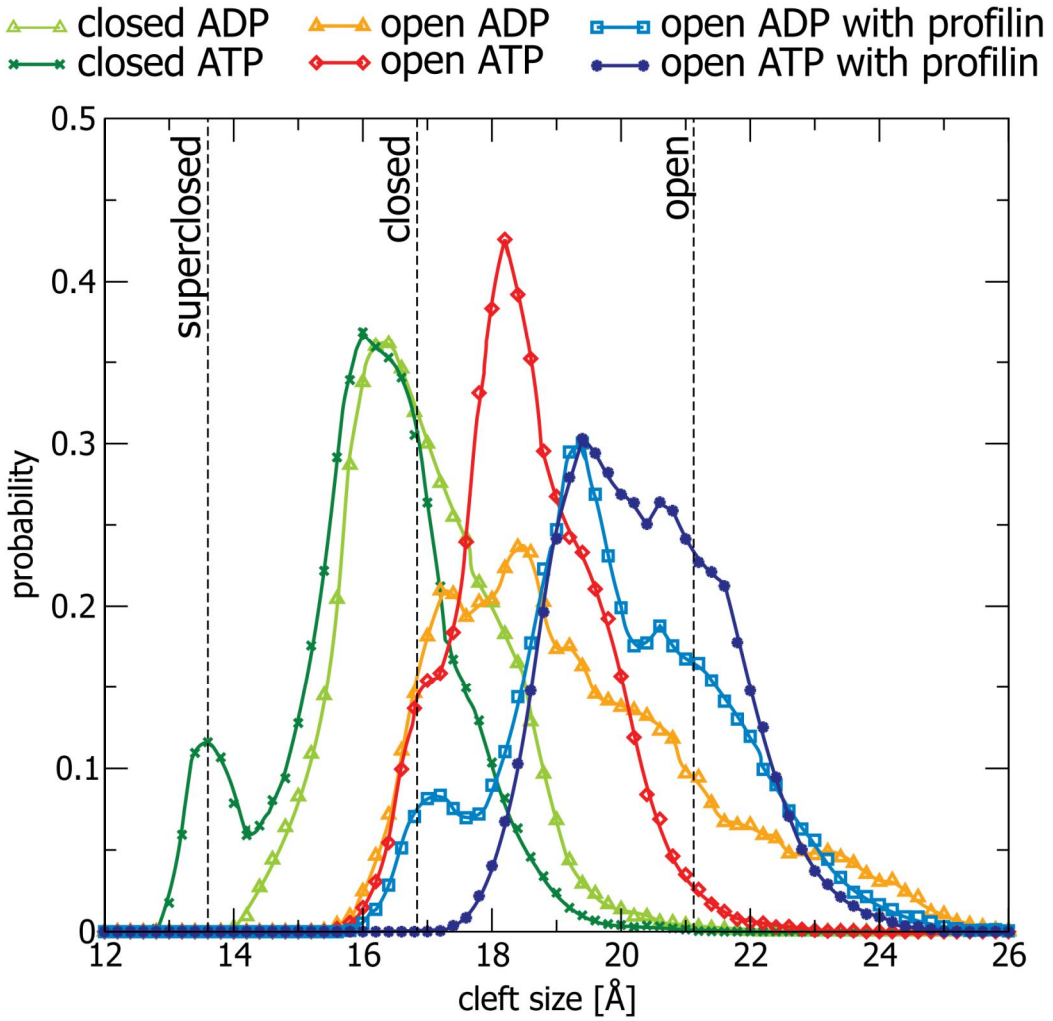

Figure 5. Probability density of the cleft size between subdomain 2 and 4 over the entire simulation time. Each open state graph represents the data of 10 simulations (20 for closed state). The vertical dashed lines indicate the cleft sizes of the crystallographic open and closed states and the average superclosed state proposed here. The cleft size distribution of profilin-bound actin (blue) appears to be broader with the main peak slightly shifted from the open state towards the closed state. The shift of the open state simulations without profilin (red) is much stronger, with the main peak being closer to the closed state than to the open state. The two closed state simulations (green) show little spread in comparison and remain in close proximity to the starting value. In the ATP-bound closed-state simulations an additional smaller peak appears at 13.7 Å corresponding to the superclosed state, that does not appear in the corresponding ADP-closed state simulations.

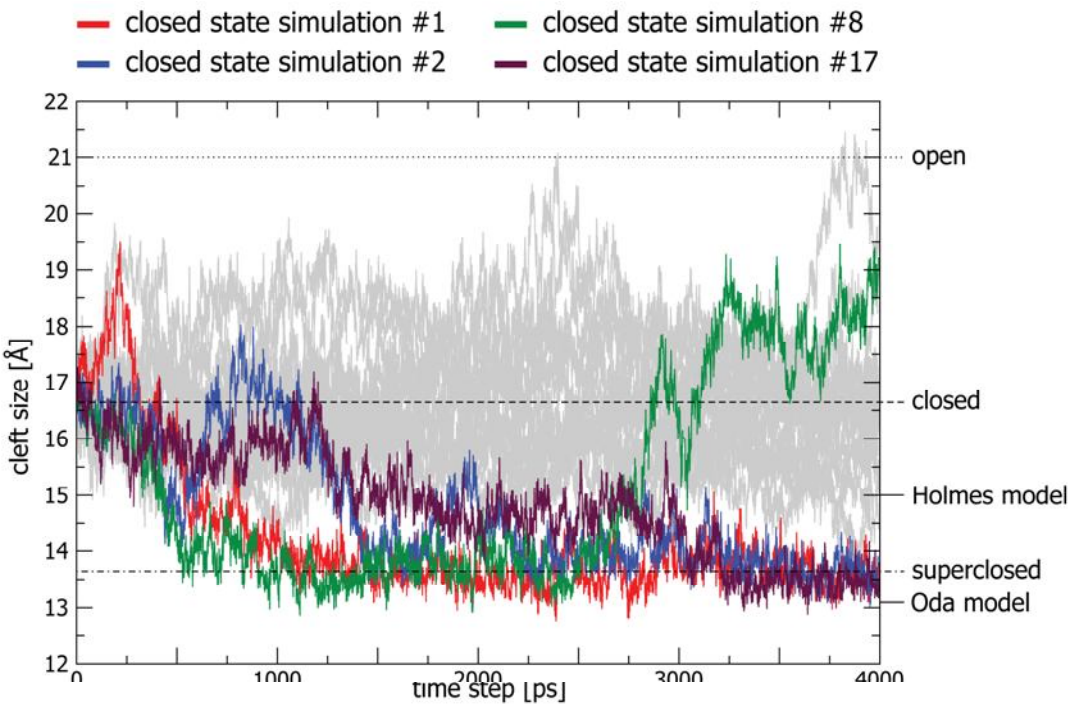

Figure 6. Time series of the cleft size of 20 MD simulations of ATP-bound actin in the closed state. The 4 simulations in which the protein structure adopts the superclosed conformation are shown in colour, the remaining simulations in grey. On the right axis the cleft sizes of the open and closed crystal structures (21.1 Å and 16.7 Å), the Holmes and Oda filament models (15 Å and 13.1 Å) and the average superclosed state (13.7 Å) are marked for comparison.

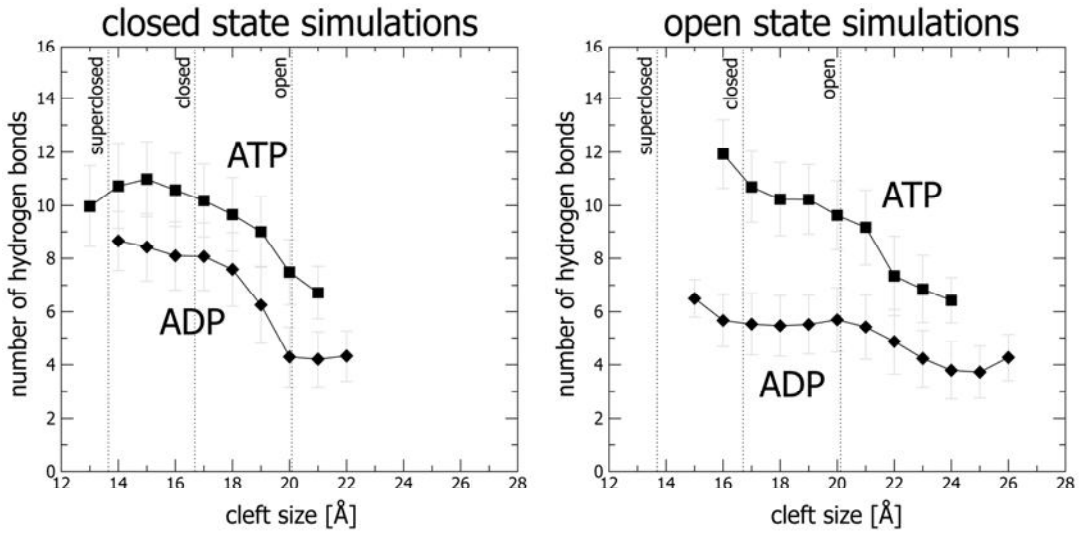

Figure 7. Average number of hydrogen bonds between nucleotide and protein plotted versus the cleft size. The left panel shows the number of hydrogen bonds averaged over the 40 simulations of the closed state and the right panel over the 20 open state simulations in absence of profilin. The bars of the data points give the standard error. In general, MD structures of actin with a smaller cleft size are accompanied by a high number of hydrogen bonds while there are fewer in open conformations. The overall low hydrogen occupancy in simulations of open state actin with ADP is attributed to the poorly hydrogen-bonded ADP in the starting structure of this simulation model, leading to a destabilisation of the tertiary structure which in turn explains the large fluctuations in cleft size.

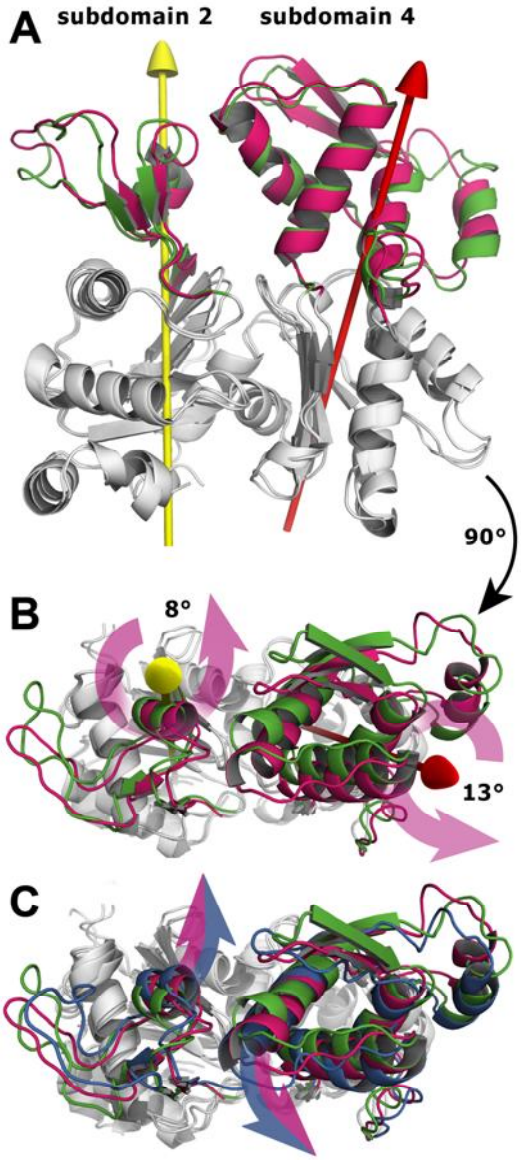

Figure 8. Comparison of the structures of the closed state (2BTF, green), the average superclosed structure (violet) and the Holmes filament model (blue).

A, B - Subdomain 1 and 3 (white) of closed and superclosed state aligned and the axes of rotation of subdomain 2 (yellow) and 4 (red) determined. The rotation angle of superclosed subdomain 2 is 8.3° and 13° for subdomain 4.

C - Superclosed state and Oda filament model aligned to the structure of the closed state, taking into account the backbone of the entire actin molecule. The purple-blue arrows indicate the rotations of subdomains 2 and 4 in the superclosed and filament model structures.

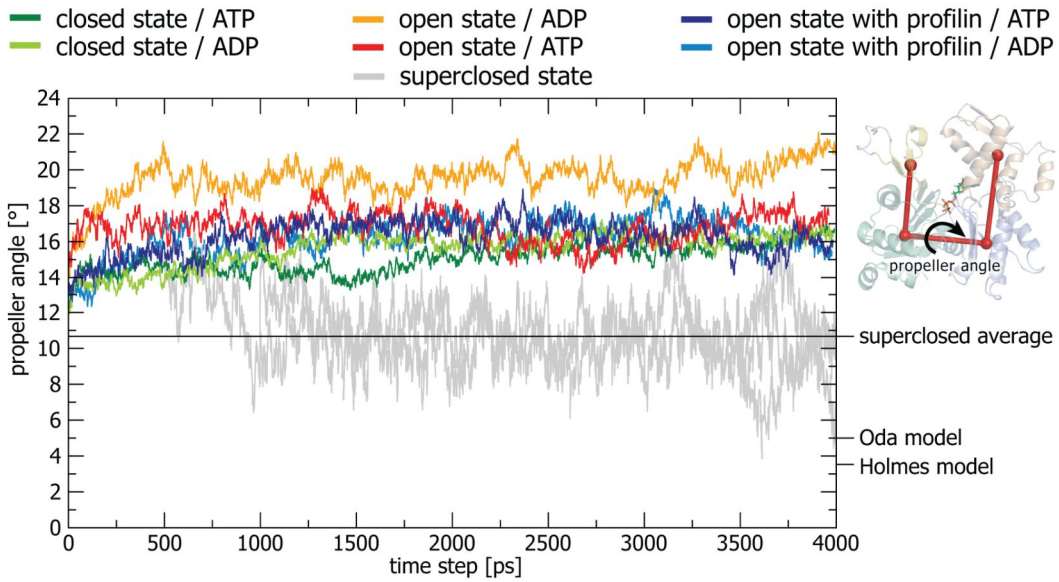

Figure 9. Time Series of propeller angles. Each graph of the open and closed state simulations represents the average over 10 and 20 simulations, respectively. The four superclosed parts of the closed state ATP-actin trajectories are shown in grey. Their average angle is 10.7° (solid line). In comparison, the angle of an actin monomer in the Oda filament model is 5° and in the Holmes filament model 3.6°.

PDB ID	Actin State	Bound Profilin	Nucleotide	System size [atoms]	Simulation time
1HLU	Open	No	ATP	77,321	10 x 4 ns
1HLU	Open	Yes	ATP	122,034	10 x 4 ns
2BTF	Closed	No	ATP	77,321	20 x 4 ns
1HLU	Open	No	ADP	77,328	10 x 4 ns
1HLU	Open	Yes	ADP	122,025	10 x 4 ns
2BTF	Closed	No	ADP	77,343	20 x 4 ns
MD-structure	superclosed	No	ATP	77,321	20 x 1 ns
MD-structure	superclosed	No	ADP	77,343	20 x 1 ns
2HF4	Closed	No	ATP	77,300	10 x 4 ns
2HF3	Closed	No	ADP	77,357	10 x 4 ns

Table 1. Overview of the models studied by MD simulation. The total simulation time is 440 ns.

Supplemental Material

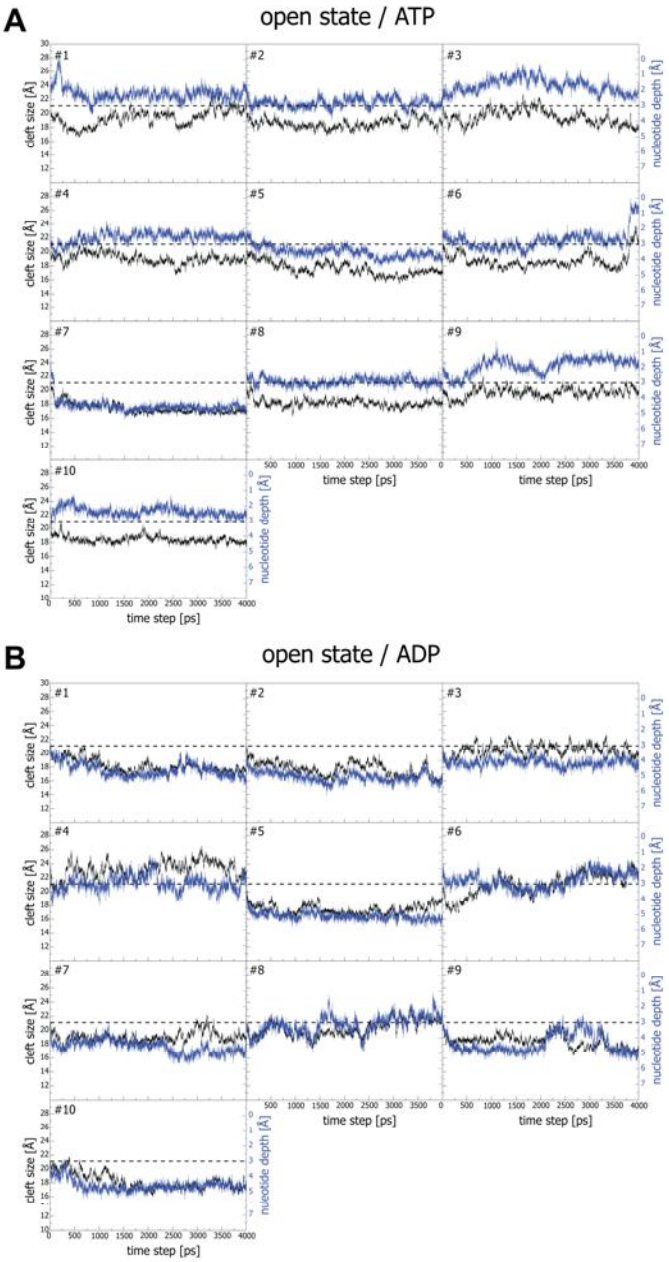

Figure 10. Time series of individual cleft size during MD simulations of the open state.

Cleft size (black) and nucleotide depth (blue) over simulation time of

A - 10 open state ADP-G-actin simulations and

B - 10 open state ATP-G-actin simulations.

The dashed line indicates the initial cleft size of the open state crystal structure.

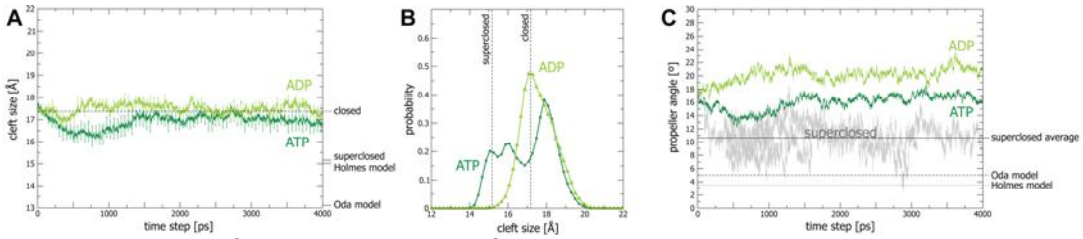

Figure 11. Results of 10 MD simulations of PDB ID 2HF4 (ATP closed state) and 2HF3 (ADP closed state).

A – Time series of the average cleft size between subdomains 2 and 4 during MD simulations of ATP- and ADP-G-actin.

B – Probability density of the cleft size between subdomain 2 and 4 over the entire simulation time.

C – Change of propeller angle over simulation time. Averages over 10 simulations each. Superclosed sections of the ATP closed simulations are shown in grey.